NON-DESTRUCTIVE OPTICAL ANALYSIS OF POROSITY CONTENT DURING Yt: YAG LASER WELDING OF Al Alloy 1050 USING X-RAY MICRO-TOMOGRAPHY

Diana CHIOIBASU[11,2], Adrian SIMA[1], Cosmin DOBREA[1], Irina PAUN[1], Andrei POPESCU[1], Catalin LUCULESCU[1], Ion TISEANU[1], Niculae PUSCAS[2]

In this study continuous laser welding of two thickness of aluminium was investigated. Aluminium A 1050 was used. Preliminary study was done to establish the power required for the material to begin to melt and one set of samples were welded in butt joint configuration. The welding was carried out using a solid state laser. The length of the samples welded was 25 mm and the width about 2 mm. Process parameters were optimized for achieving weld without porosity. In this study non-destructive control, like X ray radiography and tomography was done to analyse the defects inside the welding samples.

Keywords: laser welding, aluminium, non-destructive control, X-ray, micro-tomography

1. Introduction

Due to the many advantages and benefits that laser in manufacturing it provides lately, laser processing of materials has been increasing. To achieve objectives like fuel efficient engines and mass efficient structural materials, aiming to reduce the total weight of the vehicle, are required in automotive and aerospace [1-3]. Therefore, light alloys are increasingly in use along with the traditional structural materials in vehicle designs. Aluminium (Al) is one of the materials of choice as it is cost effective, has high specific modulus and is corrosion resistant [4]. Laser welding compared to other conventional welding process such as electron beam, gas metal arc welding, gas tungsten arc welding, etc. has high productivity, low heat input, can be weld small-thin materials, no filler metals necessary. Laser welding aluminium is quite difficult to weld due to the characteristics of aluminium-oxide forms on the aluminium. Aluminium melts at 685 degrees C and aluminium oxide melts around 2000 degrees C, so the oxide doesn`t melt during laser welding process. The oxide is porous and so will be the welding samples [5].

[1] National Institute for Laser, Plasma and Radiation Physics, Magurele Romania, email: chioibasu.georgiana@inflpr.ro
[2] Faculty of Applied Sciences, Department of Physics University POLITEHNICA of Bucharest, Romania

The properties of the weld joints depends of the defects formed during the welding process [6]. Many types of defects like gas pores, lack of fusion, micro cracks holes can occur in the welding process [7] [8] [9] [10] [11]. Process parameters are very important in this operation and it has been done optimization of laser power, laser speed and gas pressure for achieving weld without crack, pores or others defects. In this study non-destructive control, like X-ray radiography and tomography was done to analyse the defects inside the welding tests. X-ray computed tomography (XCT) is a 3D imaging technique which allows characterization of porosity in different scientific zone of research such as metal materials [12] [13] [14], medical imaging [15], biomaterials [16], composited [17], welding [18]. XCT was used to investigate the amount of porosity in various laser welded cast alloys and found out that the porosity has a big influence on tensile strength of joints [19], to determine the consequence of the process parameters on porosity formation and microstructure of Ti-6Al-4V welded by Nd:YAG laser welding [20], to examine the porosity in 316L stainless steel powders formed by selective laser welding technique [21]

2. Experimental set-up and material

The experiment was done using a laser welding system, schematically shown on figure 1. Solid state laser (TruDisk 3001, wavelength 1030 nm) with a maximal power of 3000 W CW was used. The laser beam was focused and guided by optical fiber and modular processing optics BEO D70 welding which was attached to a six-axis robot arm (TruLaser Robot 5020). The optics are presented in figure 1 and it is equipped with motor-driven focus setting procedure, which makes possible to set the focus differently for each welding seam.
Argon was used for shielding above and behind the welds. The system allows welding processing speed up to 2 m/s with positional accuracy of ± 0. 1 mm and the laser spot diameter is 600 µm. Fig. 2 shows the experimental set up used for the welding tests.

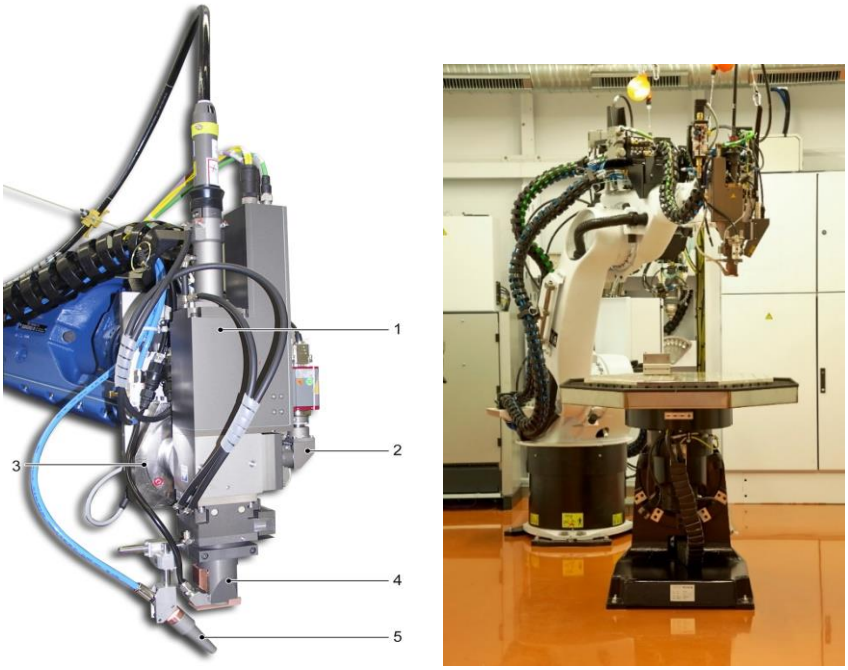

Fig. 1. TruLaser Robot equipped with Welding Processing Optics. 1 Processing optics BEO D70; 2 Monitoring camera with monitoring Software; 3 Magnetic coupling; 4 Cross-jet; 5 Inert gas nozzle

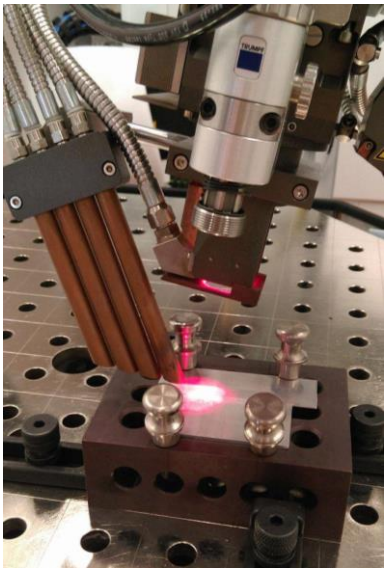

Fig.2. Experimental set-up

In the present study, the material used was A1050 aluminium alloy with two different dimension sheets, one with 120 mm x 40 mm x 1 mm and the second with

100 mm x 40 mm x 2 mm. The chemical composition and mechanical properties are presented in the Table 1. The material was cleaned with alcohol and dried at warm air before welding, in order to get best quality of welds. The rectangular specimens were clamped with magnetic pins to a welding table in a butt joint configuration. Clamping is an important factor for laser welding process, since defects like cracks and porosity can occur.

Table 1

Chemical composition of aluminium A 1050 (weight %).

Material	**Elements (wt %)**							
	Cu	Mg	Si	Fe	Mn	Zn	Ti	Al
A 1050	≤0.05	≤0.05	≤0.25	≤0.4	≤0.05	≤0.07	≤0.05	Balance

X-Ray Microtomography

X-Ray Microtomography (or micro CT) create images with cross-sections of materials using x-rays and the build a virtual 3D model [22]. It is a radiographic imaging technique nondestructive that can make 3D pictures inside of the material with resolution better than 1 micrometer. After processing data quality measurements can be obtain from the tomographic data [23]. Microtomography has applications in medicine and industrial research. The setup for industry is used the one with the X-Ray source and detector being stationary while the sample rotate. In the picture 3 is presented the setup used for welding analysis. For the present study X-ray source used has maximum high voltage: 225 kVp, feature recognition: <1 µm, minimum object-focus distance: 0.4 mm, X-Ray cone: 170°.

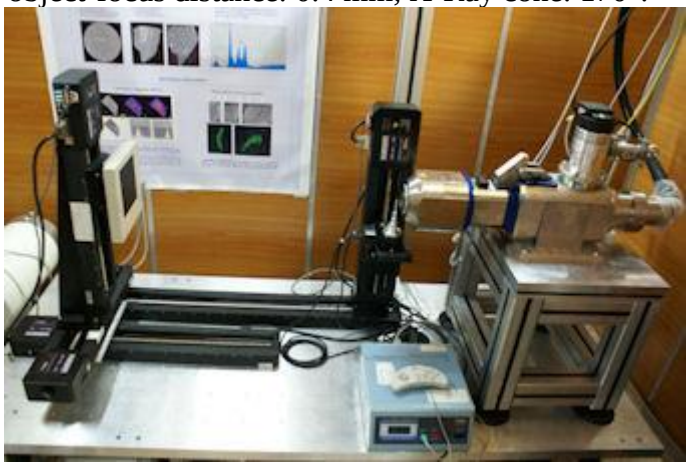

Fig. 3. Microtomography set-up

3. Results

In the laser welding process the optimization of the parameters are crucial, laser power, speed and focus are the principal parameters in this operation. Also, the gas type and pressure of the gas is an important factor to achieve a quality weld. For this experiment preliminary optimization of the parameters were carried out. To establish the values range of the power, speed and shielding gas pressure many tests were done. To determine the optimum power tests was started at 1000 W and then increase with 200 W until the material starts to weld. The laser speed was determined starting with 0.6 m/s and decreasing with 0.1 m/s until the weld become wider. Different angles of the focusing optics head were used in order to determine the optimal positioning of the shielding gas. Angle B, respective angle C is the rotation of the axis Y, respective axis Z. That is how the parameters from the table 2 were established. Because aluminium it is a very difficult material to weld, 9 tests of welding were done under different sets of parameters.

Tabel 2

Laser welding parameters

Nr. Crt.	Power [W]	Speed [m/s]	Shielding gas Ar [l/min]	Gas pressure [bar]	Focus [mm]	Angle B	Angle C
1	2000	0.03	26	1	-1	0	0
2	2000	0.03	26	1	0	0	0
3	1750	0.03	26	1	0	0	0
4	1750	0.03	26	1	-1	0	0
5	2000	0.02	6	1	-1	0	-5
6	2000	0.025	6	1	-1	0	-5
7	2000	0.025	4	1	-1	0	-5
8	2000	0.025	26	1	-1	-10	-10
9	2000	0.025	26	1	0	-10	-10

Samples were subjected to non-destructive control. X-ray radiographs were performed at 60 kV and 300 μA current, with 30 radiographs being applied. A tomography measurement for sample 2 was also performed to determine complex information about the structure and geometry of the pores in the sample. However, the radiographs were analysed first, as it is shown in the figure 4.

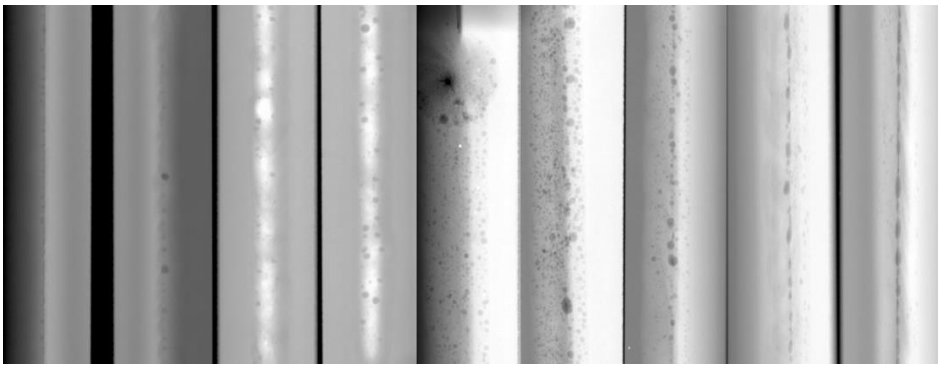

Fig.4. Radiographs on samples 1- 9 (from left to right)

In order to highlight the pores and defects, the processing images were performed by applying an FFT filter and the results are presented in the figure 5.

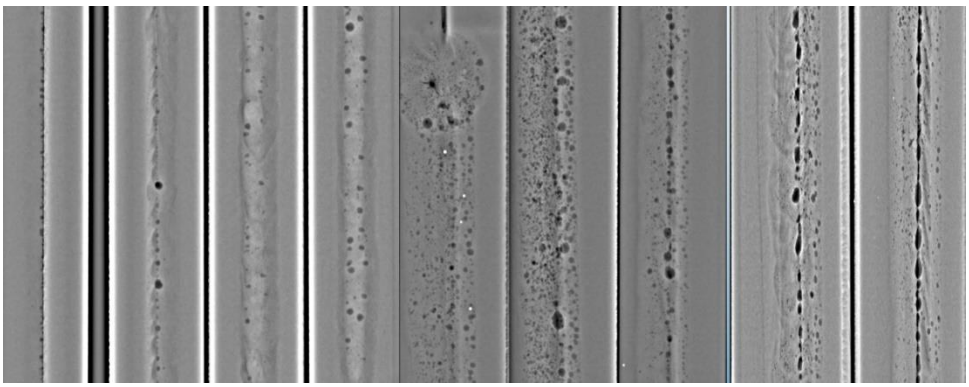

Fig.5. Radiographs on samples 1-9 filtered

Knowing exactly the size of the detector with which these radiographs and distance sources - the detector (SD) and the object source (SO) were made - the pixel size of these images was determined. Thus, for 1 to 7 radiographs we have the size of a pixel equal to 10.44 μm. In the case of radiographs 8 and 9 the object source distance changed, so the pixel size changed from 10.44 μm to 7.7 μm. It can be seen the key hole defect on the sample 5, but this has not been taken into account (detecting the pores was done under this defect).

The image processing program has passed a phase of processing these images, namely their individual selection, finding a threshold value so that can precisely select these pores and defects and can be measured.

It can be seen from these images that the welding of sample 1 was not properly realized because one can still see a channel between the two welded together duralumin plates. With this information, it was possible to determine with the ImageJ program the number of apertures on each welded sample, the average size and the minimum and maximum size of each pore. It was also possible to

calculate the total area of these pores and the percentage occupied by this area in the total area of the sample to be scanned. In the case of 8 and 9 radiographs, changing the size of the pixel (the samples being closer to the X-ray source), a greater quantity of cells could be determined as well as even major welding defects. After applying the threshold value following characteristics (table 3) were obtained for 2 to 9, because sample 1 was unable to study porosity due to the defective joint.

Table 3

Pores dimensions for samples 2-9

Sample number	Pores number	Percentage of pores area from the total area (%)
Sample 2	44	1.01%
Sample 3	52	1.001%
Sample 4	41	1.439%
Sample 5	507	10.734%
Sample 6	362	5.033%
Sample 7	224	4.344%
Sample 8	259	2.739%
Sample 9	247	3.532%

It can be observed that the sample 2 it is the best joint because even if has not the smallest number of pores, has the smallest percentage of pores area from the total area. In the figure 6 is presented a picture of the weld 2 taken by an optical microscope.

Fig. 6. Picture of the weld 2 taken by an optical microscope

In addition to these radiographs, a tomography for the number 2 sample was made, which was able to observe the geometrical structure of these pores, their placement in the studied object and the determination of their dimensions in 3 coordinates. Thus, using the VG Studio Max program, the tomographic reconstruction of the piece was performed, and the size of the selected pore could be measured (Fig. 7).

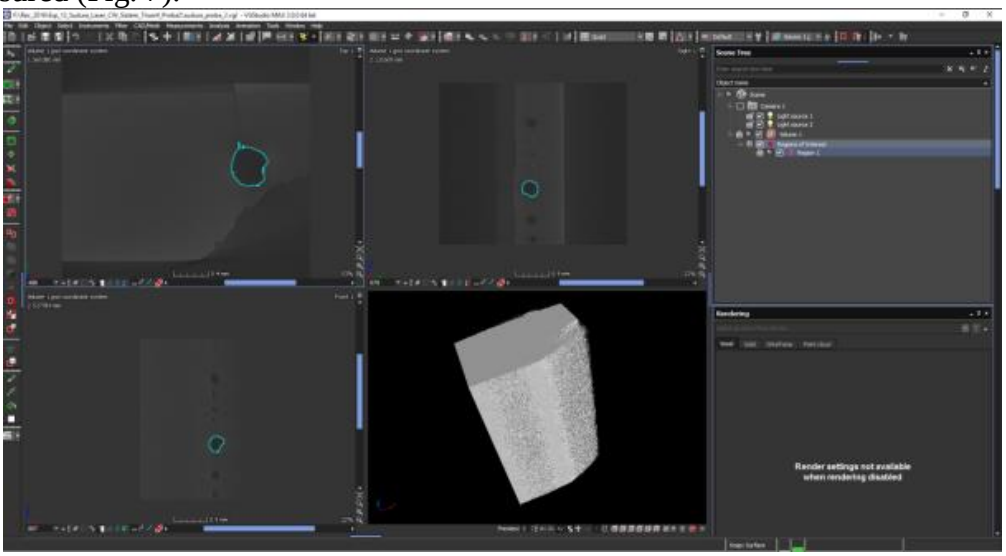

Fig. 7. 3D reconstruction of sample 2 and the selection of the region of interest

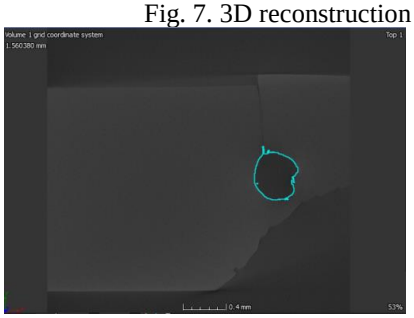

Top plan

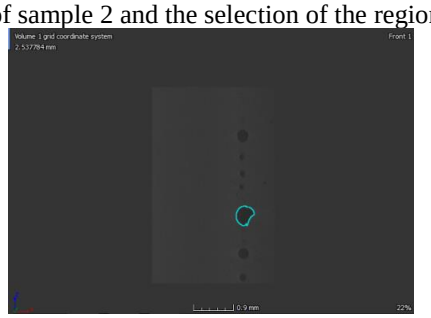

Front plan

Right plan

Fig. 8. 3D reconstruction of sample 2 in different views

For this region of interest, the following characteristics were obtained:
• Dimensions (x / y / z) - voxels: 132/167/149
• Resolution (x / y / z) - mm: 0.003143 / 0.003143 / 0.003143
• Total number of voxels: 1296586
• Total volume (mm3): 0.040247
• Dimensions (x / y / z) - mm: 0.414845 / 0.524842 / 0.468271

4. Conclusions

The defects inside the welding experiments were analysed using non-destructive control like X-ray radiography and for the weld with the fewer pores, tomography was done to study the geometry and dimensional structure of the pores. Optimization of the principal parameters, like laser power, laser speed and gas pressure was studied. The best weld was achieved using 2000 W laser power, 0.3 m/s laser speed and 26 l/min shielding gas. This sample has the percentage of pores area from the total area 1% It can be observed that if the laser speed is lower the pores number increase, because there is a much more material it melts and easily many particles of gas get inside the weld and the material solidifies with pores.

REFERENCES

[1]. *X. Tan, Y. Kok, Y.J. Tan, M. Descoins, D. Mangelinck, S.B. Tor, et al,* Graded microstructure and mechanical properties of additive manufactured Ti–6Al–4V via electron beam melting, Acta Materialia, **vol 97**, September 2015, pp. 1-16

[2]. *N. Arivazhagan, S. Singh, S. Prakash, G.M. Reddy,* Investigation on AISI 304 austenitic stainless steel to AISI 4140 low alloy steel dissimilar joints by gas tungsten arc, electron beam and friction welding Materials and design, **vol 32**, May 2011, pp. 3036-3050

[3]. *Y.C. Chen, D. Bakavos, A. Gholinia, P.B. Prangnell,* HAZ development and accelerated post-weld natural ageing in ultrasonic spot welding aluminium 6111-T4 automotive sheet, Acta Materialia, **vol 60**, April 2012, pp. 2816-2828

[4]. *S. Meco, G. Pardal, S. Ganguly, S. Williams, N. McPherson,* Application of laser in seam welding of dissimilar steel to aluminium joints for thick structural components, Optics and Lasers in Engineering, **vol 67**, October 2014, pp. 22-30

[5]. *F. Armao*, Aluminum Workshop: Why it's so hard to weld anodized aluminium practical welding today january / february 2015,
http://www.thefabricator.com/article/aluminumwelding/aluminum-workshop-why-it-s-so-hard-to-weld-anodized-aluminum

[6]. *M. Potesser, T. Schoeberl, H. Antrekowitsch, J.* Bruckner, The Characterization of the Intermetallic Fe-Al Layer of Steel-Aluminum Weldings, EPD Congress, March 2006, pp. 167-176

[7]. *M. Sheikhi, F. Malek Ghaini, H. Assadi*, Prediction of solidification cracking in pulsed laser welding of 2024 aluminum alloy, Acta Materialia, **vol 82**, January 2015, pp. 491–502

[8]. *T. Yuan, X. Chai, Z. Luo, S. Kou* "Predicting susceptibility of magnesium alloys to weld-edge cracking, Acta Materialia, **vol 90**, May 2015, pp. 242-251

[9]. *S. Kou*, A criterion for cracking during solidification, Acta Materialia, **vol 88**, April 2015, pp. 366-374

[10]. *H. Park, M. Choi, J. Park, W. Kim*, A study on detection of micro-cracks in the dissimilar metal weld through ultrasound infrared thermography, Infrared Physics and Technology, **vol 62**, January 2014, pp. 124-131
[11]. *I. Valavanis, D. Kosmopoulos*, Multiclass defect detection and classification in weld radiographic images using geometric and texture features, Expert Systems with Applications, **vol 37**, December 2010, pp. 7606-7614
[12]. *M. De Giovanni, J.M. Warnett, M.A. Williams, N. Haribabu, P. Srirangam*, X-ray tomography investigation of intensive sheared Al–SiC metal matrix composites, Materials Characterization, **vol 110**, December 2015, pp. 258-263
[13]. *B. Cai, S. Karagadde, L. Yuan, T.J. Marrow, T. Connolley, P.D. Lee*, In situ synchrotron tomographic quantification of granular and intragranular deformation during semi-solid compression of an equiaxed dendritic Al–Cu alloy, Acta Materialia, **vol 76**, September 2014, pp. 371-380
[14]. *S. Karagadde, P.D. Lee, B. Cai, J.L. Fife, M.A. Azeem, K.M. Kareh*, Transgranular liquation cracking of grains in the semi-solid state, Nature Communication, **vol 6**, August 2015
[15]. *A.M. Korsunsky, N. Baimpas, X. Song, J. Belnoue, F. Hofmann, B. Abbey*, Strain tomography of polycrystalline zirconia dental prostheses by synchrotron X-ray diffraction, Acta Materialia, **vol 59**, April 2011, pp. 2501-2513
[16]. *A.C. Jones, C.H. Arns, A.P. Sheppard, D.W. Hutmacher, B.K. Milthorpe, M.A. Knackstedt*, Assessment of bone ingrowth into porous biomaterials using MICRO-CT, Biomaterials, **vol 28**, May 2007, pp. 2491-2504
[17]. *J. Riesch, J.Y. Buffiere, T. Höschen, M. Di Michiel, M. Scheel, C. Linsmeier*, In situ synchrotron tomography estimation of toughening effect by semi-ductile fibre reinforcement in a tungsten-fibre-reinforced tungsten composite system, Acta Materialia, **vol 61**, November 2013, pp. 7060-7071
[18]. *M. Peel, A. Steuwer, M. Preuss, P.J. Withers*, Microstructure, mechanical properties and residual stresses as a function of welding speed in aluminium AA5083 friction stir welds, Acta Materialia, **vol 51**, September 2003, pp. 4791-4801
[19]. *R. Nomoto, Y. Takayama, F. Tsuchida, H. Nakajima*, Non-destructive three-dimensional evaluation of pores at different welded joints and their effects on joints strength, Dental Materials, **vol 26**, December 2010, pp. e246-e252
[20]. *X.L. Gao, L.J. Zhang, J. Liu, J.X. Zhang*, Porosity and microstructure in pulsed Nd:YAG laser welded Ti6Al4V sheet, Journal of Materials Processing Technology, **vol 214**, July 2014, pp. 1316-1325
[21]. *G. Ziółkowski, E. Chlebus, P. Szymczyk, J. Kurzac*, Application of X-ray CT method for discontinuity and porosity detection in 316 L stainless steel parts produced with SLM technology, Archives of Civil and Mechanical Engineering, **vol 4**, August 2014, pp. 2-8
[22]. Wikipedia https://en.wikipedia.org/wiki/X-ray_microtomograph Accessed on 02/06/2017
[23]. *Eric N. Landisa, Denis T. Keaneb*, X-ray microtomography, Materials Characterization, **vol 61**, September 2010, pp. 1305-1316